

1 **Influence of ruthenium doping on UV- and visible-light**  
2 **photoelectrocatalytic color removal from dye solutions**  
3 **using a TiO<sub>2</sub> nanotube array photoanode**

4 Patricia García-Ramírez <sup>a</sup>, Erik Ramírez-Morales <sup>b</sup>, Juan Carlos Solis Cortazar <sup>c</sup>,  
5 Ignasi Sirés <sup>d,\*</sup>, Susana Silva-Martínez <sup>e,\*\*</sup>

6 *<sup>a</sup> Posgrado de Doctorado en Ingeniería y Ciencias Aplicadas, Centro de Investigación en*  
7 *Ingeniería y Ciencias Aplicadas, Universidad Autónoma del Estado de Morelos. Av.*  
8 *Universidad 1001, Col. Chamilpa, Cuernavaca, Morelos C.P. 62209, Mexico*

9 *<sup>b</sup> División Académica de Ingeniería y Arquitectura, Universidad Juárez Autónoma de Tabasco,*  
10 *Av. Universidad S/N, Col. Magisterial, C.P. 86040, Villahermosa, Tabasco, Mexico*

11 *<sup>c</sup> Posgrado en Ciencias en Ingeniería, Universidad Juárez Autónoma de Tabasco, Av.*  
12 *Universidad S/N, Col. Magisterial, C.P. 86040, Villahermosa, Tabasco, Mexico*

13 *<sup>d</sup> Laboratori d'Electroquímica dels Materials i del Medi Ambient, Departament de Química*  
14 *Física, Facultat de Química, Universitat de Barcelona, Martí i Franquès 1-11, 08028*  
15 *Barcelona, Spain*

16 *<sup>e</sup> Centro de Investigación en Ingeniería y Ciencias Aplicadas, Universidad Autónoma del*  
17 *Estado de Morelos. Av. Universidad 1001, Col. Chamilpa, C.P. 62209, Cuernavaca, Morelos,*  
18 *Mexico*

19 *\*Corresponding author's e-mail address: i.sires@ub.edu (I. Sirés)*

20 *\*\*Corresponding author's e-mail address: ssilva@uaem.mx (S. Silva-Martínez)*

21 **Abstract**

22 The photocatalytic activity of TiO<sub>2</sub> anodes was enhanced by synthesizing Ru-doped Ti|TiO<sub>2</sub>  
23 nanotube arrays. Such photoanodes were fabricated via Ti anodization followed by Ru  
24 impregnation and annealing. The X-ray diffractograms revealed that anatase was the main TiO<sub>2</sub>  
25 phase, while rutile was slightly present in all samples. Scanning electron microscopy evidenced  
26 a uniform morphology in all samples, with nanotube diameter ranging from 60 to 120 nm. The  
27 bias potential for the photoelectrochemical (PEC) treatment was selected from the  
28 electrochemical characterization of each electrode, made via linear sweep voltammetry. All the  
29 Ru-doped TiO<sub>2</sub> nanotube array photoanodes showed a peak photocurrent (PP) and a saturation  
30 photocurrent (SP) upon their illumination with UV or visible light. In contrast, the undoped  
31 TiO<sub>2</sub> nanotubes only showed the SP, which was higher than that reached with the Ru-doped  
32 photoanodes using UV light. An exception was the Ru(0.15 wt.%) -doped TiO<sub>2</sub>, whose SP was  
33 comparable under visible light. Using that anodes, the activity enhancement during the PEC  
34 treatment of a Terasil Blue dye solution at  $E_{\text{bias}}(\text{PP})$  was much higher than that attained at  
35  $E_{\text{bias}}(\text{SP})$ . The percentage of color removal at 120 min with the Ru(0.15 wt.%) -doped TiO<sub>2</sub> was  
36 98% and 55% in PEC with UV and visible light, respectively, being much greater than 82%  
37 and 28% achieved in photocatalysis. The moderate visible-light photoactivity of the Ru-doped  
38 TiO<sub>2</sub> nanotube arrays suggests their convenience to work under solar PEC conditions, aiming  
39 at using of a large portion of the solar spectrum.

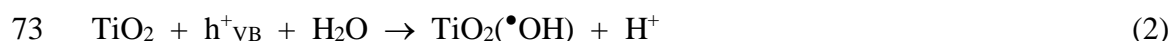
40 *Keywords:* Bias potential; Doped TiO<sub>2</sub>; Hydroxyl radical; Organic pollutant;  
41 Photoelectrocatalysis; Water treatment

## 42 **1. Introduction**

43 The occurrence of organic pollutants in the aquatic ecosystems, even at low concentrations,  
44 has derived in emerging environmental concerns on a global scale, owing to their high toxicity  
45 and usual persistence (Choo et al., 2020). The advanced oxidation processes (AOPs) have  
46 progressed as a diverse group of technologies whose most characteristic feature is the ability to  
47 generate powerful oxidant species like hydroxyl radical ( $\cdot\text{OH}$ ) (Brillas et al., 2009). A high  
48 mineralization degree, i.e., transformation of the organic molecules into inorganic ions,  $\text{CO}_2$   
49 and  $\text{H}_2\text{O}$  is feasible, which ensures the gradual detoxification of the polluted effluents (Oturán  
50 and Aaron, 2014). Note that, among the different families of organic pollutants in water, dyes  
51 are particularly troublesome because they cause high aesthetic impact even at trace  
52 concentrations. Furthermore, dyes and their N-derivatives formed upon hydrolysis and natural  
53 photo or biotransformation have been linked to carcinogenic and mutagenic effects. There exist  
54 more than 100,000 commercially available dyes, and about 280,000 tons of textile dyestuff are  
55 discharged into aqueous streams every year because of their massive use in many industrial  
56 processes (Brillas and Martínez-Huitle, 2015). The electrochemical advanced oxidation  
57 processes have shown great effectiveness for water decolorization, in particular electro-  
58 oxidation (EO) (Clematis et al., 2017), electro-Fenton (Thiam et al., 2015; Vasconcelos et al.,  
59 2016) and photoelectrocatalysis (PEC) (Espinola-Portilla et al., 2017; Oriol et al., 2019).

60 The great effectiveness of AOPs like heterogeneous photocatalysis (PC) and EO, as well  
61 as Fenton-, ozone- and ultrasound-based processes and their combinations for the degradation  
62 of organic contaminants in water and wastewater has been demonstrated (Martínez-Huitle et  
63 al., 2015; Zhu et al., 2019; Anandan et al., 2020; Cornejo et al., 2020; Kanan et al., 2020).  
64 Among such processes, PC with  $\text{TiO}_2$  powder as photoactive material has been widely  
65 investigated for water treatment, since the procedure is simple and this photocatalyst exhibits  
66 high photochemical stability and photoactivity, low cost and non-toxicity (Kanan et al. 2020).

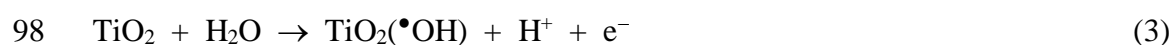
67 Upon irradiation with UV photons ( $\lambda < 387$  nm), whose energy is greater than the TiO<sub>2</sub> bandgap  
68 ( $E_{\text{gap}} = 3.2$  eV for anatase structure) (Yan et al., 2013), the electrons jump out from the valence  
69 band (VB) of the semiconductor to its conduction band (CB). This results in the generation of  
70 a hole ( $h^+_{\text{VB}}$ ) and an electron ( $e^-_{\text{CB}}$ ) as charge carriers, according to reaction (1). Water can then  
71 be oxidized by the  $h^+_{\text{VB}}$  to form adsorbed  $\bullet\text{OH}$  at the TiO<sub>2</sub> surface via reaction (2).



74 However, PC with raw TiO<sub>2</sub> powder shows three main drawbacks: (i) the poor  
75 photoactivity under visible light, (ii) the high recombination rate of the photoinduced  $e^-_{\text{CB}}/h^+_{\text{VB}}$   
76 pairs, and (iii) the additional cost required to recover the suspended TiO<sub>2</sub> particles at the end of  
77 the treatment (Zhang et al., 2012; Basavarajappa et al., 2020). To overcome these limitations,  
78 modified TiO<sub>2</sub> has been developed and supported on different substrates. The surface  
79 modification aims to achieve a narrower bandgap, thus promoting the absorption of visible light  
80 and decreasing the recombination rate of carriers (Hernández et al., 2018; Basavarajappa et al.,  
81 2020; Chen et al., 2020). Among the dopant species with proven effectiveness, ruthenium can  
82 reduce the  $E_{\text{gap}}$  of TiO<sub>2</sub> to allow the visible-light-driven PC, and it also acts as electron  
83 donor/acceptor, which efficiently minimizes the recombination because the electron transfer is  
84 accelerated (Nguyen-Phan et al., 2016; Ismael, 2019). Ru-doped TiO<sub>2</sub> nanotubes have been  
85 used for the oxidation of organic pollutants by PC under UV or visible light (Wang et al., 2016;  
86 González et al., 2019). Other applications include visible-light water splitting (Ohno et al.,  
87 1999) hydrogen production (Nguyen-Phan et al., 2016), sensors (Viswanathamurthi et al.,  
88 2004) and dye-sensitized solar cells (So et al., 2012).

89 Alternatively, the reduction of the  $e^-_{\text{CB}}/h^+_{\text{VB}}$  recombination can become more significant  
90 in the PEC process. It consists in the application of a rather small bias (i.e., anodic) potential

91 ( $E_{\text{bias}}$  or  $E_{\text{an}}$ ) to the illuminated photoanode, which is fabricated with raw or modified  $\text{TiO}_2$   
92 nanostructures over a conductive substrate. This favors the spatial separation of both charge  
93 carriers, since the  $e^-_{\text{CB}}$  are immediately transported to the cathode of the cell (Daghrir et al.,  
94 2012; Bessegato et al., 2015; Peleyeju and Arotiba, 2018; Oriol et al., 2019). A greater  
95 decontamination efficiency can thus be attained because of the larger amount of  $\text{TiO}_2(\bullet\text{OH})$   
96 production from reaction (2), which adds to its simultaneous generation via direct water  
97 oxidation reaction (3) on the  $\text{TiO}_2$  surface (Changanaqui et al., 2020).



99       Therefore, the combination of  $\text{TiO}_2$  modification with  $E_{\text{bias}}$  application in PEC may lead to  
100 a larger accumulation of hydroxyl radicals and holes under visible light as compared to PC,  
101 thereby upgrading the oxidation of the organic contaminants (Daghrir et al., 2012; Peleyeju and  
102 Arotiba, 2018). In this work, undoped and Ru-doped  $\text{TiO}_2$  nanotube array photoanodes have  
103 been synthesized for water treatment. To our knowledge, this doped material has never been  
104 tested as photoanode for this purpose; only the binary oxide anodes ( $\text{TiO}_2\text{-RuO}_2$ ) have been  
105 investigated (Shin et al., 2013). Here, the characteristics and photoactivity of the photoanodes  
106 have been assessed, analyzing the effect of UV and visible light. A Terasil Blue dye solution  
107 (0.011 mM) was electrolyzed under PEC conditions to study the influence of key parameters  
108 like the annealing temperature for Ru doping, the applied  $E_{\text{bias}}$  and the pH of the dye solution  
109 on the color removal efficiency.

110

## 111 **2. Materials and methods**

### 112 *2.1. Chemicals and materials*

113       Ethylene glycol (98%), ammonium fluoride, sodium sulfate, sodium hydroxide,  
114 ammonium hydroxide, sulfuric acid, ruthenium(III) chloride hydrate, ethanol, acetone and other

115 chemicals employed for analysis, all of them of analytical grade, were purchased from Sigma-  
116 Aldrich and used as received. A local textile company provided Terasil Blue 3RL (1,5-  
117 Diaminobromo-4,8-dihydroxyanthraquinone, Color Index Disperse Blue 56,  $C_{14}H_9BrN_2O_4$ ,  
118 CAS No. 31810-89-6;  $M_w = 349.13$  g/mol, 150% depth shade). Titanium foil (99.6% purity,  
119 0.2 mm thickness) and Pt mesh were acquired from Sigma Aldrich. All the analytical solutions  
120 were prepared with ultrapure water.

## 121 2.2. *Synthesis of undoped and Ru-doped TiO<sub>2</sub> nanotube arrays*

122 The Ti foil substrates (2 cm × 1 cm, 0.2 mm thick) were mirror polished with abrasive sand  
123 paper of different grain sizes, washed with soapy distilled water in an ultrasonic bath  
124 (Ultrasonic Power Corporation, model 5300) for 15 min and then successively rinsed with  
125 ethanol and acetone. The Ti|TiO<sub>2</sub> nanotube arrays were synthesized by means of the Ti  
126 anodization method in an aqueous organic electrolyte. The process was carried out in a two-  
127 electrode polycarbonate electrochemical cell that contained 40 mL of 0.5 wt.% NH<sub>4</sub>F + 10 wt.%  
128 ultrapure water in ethylene glycol. A cell voltage ( $E_{cell}$ ) of 50 V was applied with a Matrix MPs-  
129 6005L-1 DC power supply between the pretreated Ti anode and a Pt mesh for 60 min. The  
130 resulting Ti|TiO<sub>2</sub> nanotubes, with a geometric active area of 1.0 cm<sup>2</sup>, were rinsed with distilled  
131 water and soaked in a 0.1 M NaOH solution for 30 min. The pieces were subsequently washed  
132 with water, dried at room temperature and finally annealed at 600 °C for 120 min.

133 To synthesize the Ru-doped TiO<sub>2</sub> nanotube arrays, a concentrated Ru(III) solution in 0.1  
134 M HCl was prepared and stirred for 180 min, filtered to remove the precipitated solid, dried at  
135 100 °C for 60 min and cooled down to room temperature in a desiccator until constant weight  
136 was attained. This procedure allowed assessing the mass of Ru(III) dissolved in the acidic  
137 medium. The solutions for Ru doping contained 0.005, 0.02, 0.04, 0.08, 0.10 and 0.15 wt.%  
138 Ru. The previously heated Ti|TiO<sub>2</sub> nanotube arrays were doped according to the following  
139 impregnation method: 400 μL of each impregnation solution were placed onto a Ti|TiO<sub>2</sub>

140 sample, followed by drying at room temperature for 48 h; then, the samples were immersed in  
141 a 0.1 M  $\text{NH}_4\text{OH}$  solution for 5 min, followed by rinsing with distilled water, drying at room  
142 temperature and annealing at 200 °C for 2 h. This temperature was lower than that causing the  
143 phase transformation of  $\text{TiO}_2$  anatase and thus, the  $\text{TiO}_2$  nanotubes structure was kept unaltered.  
144 Another set of Ru-doped  $\text{TiO}_2$  samples was prepared using the optimum Ru content (i.e., 0.15  
145 wt.%) and using different annealing temperatures (200, 450 and 600 °C) to observe the  
146 influence of this parameter on the photocatalytic activity.

### 147 *2.3. Photoanode characterization*

148 The morphology of the undoped and Ru-doped  $\text{TiO}_2$  nanotube arrays was analyzed by  
149 scanning electron microscopy employing a JEOL JSM-6010LA microscope. The crystal  
150 structures were assessed on an X-ray diffractometer (Bruker D2 PHASER, second generation),  
151 obtaining the spectra within the  $2\theta$  range of 20-70° with a grazing incidence angle of 0.5°. The  
152 Raman spectroscopy analysis was made with an XploRA Plus confocal Raman microscope ( $\lambda$   
153 = 532 nm) from Horiba Scientific. The optical bandgap energies of the nanotube arrays were  
154 obtained by diffuse reflectance UV/Vis spectroscopy, employing a Shimadzu UV2600  
155 spectrophotometer. The electrochemical/photoelectrochemical characterization of the undoped  
156 and Ru-doped  $\text{TiO}_2$  was carried out by means of linear sweep voltammetry. For this, a three-  
157 electrode quartz electrochemical cell (6 cm high, 3 cm in diameter) that contained a 0.050 M  
158  $\text{Na}_2\text{SO}_4$  solution at different pH values (1.0, 7.0 or 9.0) was employed. The anode or photoanode  
159 (working electrode), a Pt mesh (counter electrode) and  $\text{Ag}|\text{AgCl}$  (3 M KCl) as reference  
160 electrode were connected to a BASi Epsilon model E2 potentiostat interfaced with a computer  
161 to record the current (i.e., with the anode in the dark) or photocurrent (i.e., under illumination  
162 of the photoanode with UV or visible light) as a function of the applied potential (positive scan  
163 from -0.3 or -0.5 V up to 1.0 V vs the reference electrode, at a scan rate of 10 mV/s). The UV-  
164 C irradiation ( $\lambda = 254$  nm) came from a quartz-jacketed mercury Pen-Ray lamp (model 11SC-

165 1) from Analytik Jena that was submerged 4.5 cm into the solution. The visible light came from  
166 sources placed outside the solution: (i) two Ultra Plus PL-3U-25W LED lamps, or (ii) a 50 W  
167 halogen MR16 LED smart bulb. All experiments were carried out inside a black wooden box  
168 to prevent light interference from surroundings.

#### 169 2.4. Photocatalytic and photoelectrocatalytic degradation trials

170 The degradation and photodegradation ability of the undoped and Ru-doped TiO<sub>2</sub> nanotube  
171 arrays was evaluated by treating 20 mL of 0.011 mM Terasil Blue dye solution in 0.050 M  
172 Na<sub>2</sub>SO<sub>4</sub> for 120 min under PC and PEC conditions. The experiments were performed in the  
173 same 3-electrode cell described in the previous subsection. The PC trials were made simply by  
174 turning on the lamp (see UV and visible-light lamps mentioned above), keeping the potentiostat  
175 turned off. The PEC assays were executed in a similar manner, but an  $E_{\text{bias}}$  selected from the  
176 electrochemical characterization data was simultaneously applied to the anode.

177 The decolorization of the dye solution was monitored from the decay of the initial solution  
178 absorbance ( $A_0$ ) down to decreasing absorbance values as the treatment time progressed ( $A_t$ ),  
179 which was measured spectrophotometrically at the peak wavelength ( $\lambda_{\text{max}} = 552$  nm). The  
180 samples were conveniently diluted before analysis to fulfill the Lambert Beer's law. From these  
181 data, the percentage of color removal was determined as follows (Thiam et al., 2015):

$$182 \quad \% \text{ Color removal} = \frac{A_0 - A_t}{A_0} 100 \quad (4)$$

### 183 3. Results and discussion

#### 184 3.1. Characterization of the undoped and Ru-doped TiO<sub>2</sub> nanotube arrays

185 Fig. 1 shows the SEM micrographs of the undoped Ti|TiO<sub>2</sub> (Fig. 1a) nanotube arrays  
186 obtained upon calcination at 600 °C, as well as those of the Ru-doped Ti|TiO<sub>2</sub> (Fig. 1b-g for Ru  
187 content increasing from 0.05 to 0.15 wt.%) annealed at 200 °C. The anodization procedure

188 ensured the formation of well-defined and uniformly distributed nanotubes, whose internal  
189 diameter ranged from 60 to 120 nm. It is worth noting that the average diameter became slightly  
190 smaller as the Ru content in the impregnation solution was increased. The average nanotube  
191 length was  $\sim 3.42 \mu\text{m}$ . Ru atoms were uniformly distributed on the surface, without modifying  
192 the morphology of the nanotube arrays.

193 Fig. 2 shows the XRD patterns of the doped and Ru-doped Ti|TiO<sub>2</sub> nanotube arrays. In all  
194 cases, the as-prepared TiO<sub>2</sub> was calcined at 600 °C, whereas the Ru impregnation was always  
195 followed by an annealing step at 200 °C. Characteristic Ti and TiO<sub>2</sub> diffraction peaks can be  
196 identified in all samples, whereas no peak associated to metallic Ru or RuO<sub>2</sub> was found. The  
197 presence of Ti is expected from the insufficient anodization of some minor spot on the substrate  
198 employed. The absence of ruthenium species can be attributed to the low Ru content in the  
199 impregnation solution and hence, on the nanotube arrays surface (Senthilnathan et al., 2010;  
200 Ismael, 2019). Note that the absence of the dopants in the XRD patterns of modified oxides is  
201 quite typical (Chahmana et al., 2009). As evidenced in Fig. 2, the predominant crystal structure  
202 of the TiO<sub>2</sub> nanotube arrays was anatase, being the rutile phase rather undetected in all samples.  
203 This finding agrees with the reported literature that suggests the prevalence of the anatase phase  
204 over rutile as the undoped and doped TiO<sub>2</sub> nanostructures are annealed at 550 °C (Wang et al.,  
205 2016). An important finding is, therefore, that Ru doping did not interfere in the formation of  
206 the specific TiO<sub>2</sub> crystal structures expected at the heating temperatures employed, in  
207 agreement with other authors (Senthilnathan et al., 2010; Wang et al., 2016).

208 The absence of a clear rutile diffraction peak is also in agreement with the Raman spectra  
209 of the undoped and Ru-doped (annealed at 200 °C) TiO<sub>2</sub> photoanode arrays depicted in Fig. 3.  
210 In all cases, a peak with a very small intensity at a Raman shift of  $234.3 \text{ cm}^{-1}$  corresponding to  
211 rutile phase formed upon calcination at 600 °C can be identified. Secundino-Sánchez et al.  
212 (2019) observed the same Raman shift at  $234.3 \text{ cm}^{-1}$ , which was attributed to a multi-phonon

213 process in the rutile phase obtained at 600 °C. A close Raman shift, at 235.5 cm<sup>-1</sup>, has also been  
214 assigned to rutile phase (Ma et al., 2007).

215 In the Raman spectra of Fig. 3, the characteristic peaks of TiO<sub>2</sub> anatase at vibrational  
216 frequencies of 140.0, 196.6, 394.0, 518.5 and 638.7 cm<sup>-1</sup> can be distinguished, in full agreement  
217 with values reported elsewhere (Arsov et al., 1991; Ma et al., 2007; Secundino-Sánchez et al.,  
218 2019). These authors have also reported five characteristic peaks assigned to rutile phase, at  
219 Raman shifts of 141.0, 235.2, 444.5, 610.5 and 825.8 cm<sup>-1</sup> (i.e., average values calculated from  
220 the latter references). As commented above, in Fig. 3 only a single peak at 234.3 cm<sup>-1</sup> could be  
221 attributed to rutile, the rest of its typical Raman shifts being missing because of its low content  
222 on the surface. Note that the Raman spectra for the Ru-doped TiO<sub>2</sub> samples exhibited exactly  
223 the same peaks found for the undoped TiO<sub>2</sub>. Therefore, there was no influence of the Ru  
224 presence or content on the peak position of the vibrational modes.

225 The UV/Vis diffuse reflectance spectroscopy was used to determine the bandgap energies  
226 of all the synthesized materials (Fig. S1). From the reflectance spectra illustrated in the inset of  
227 Fig. S1, the  $[F(R)*hv]^{1/2}$  vs energy profiles for the undoped and Ru-doped (from 0.005 to 0.15  
228 wt.% Ru in the impregnation solution) TiO<sub>2</sub> nanotube arrays were obtained. According to the  
229 Kubelka-Munk method (López and Gómez, 2012; Nair et al., 2017), the  $E_g$  value was then  
230 estimated in each case from the intercept of the tangent with the x-axis of that main plot of Fig.  
231 S1. The undoped TiO<sub>2</sub> showed the highest  $E_g$  value (i.e., the lowest  $\lambda$ ), corroborating the idea  
232 that the photocatalyst modification is necessary to shift its absorption wavelength toward the  
233 visible range. The general trend was that the  $E_g$  decreased as the Ru content was increased,  
234 which means that the absorption band edge of all Ru-doped TiO<sub>2</sub> samples underwent a certain  
235 red-shift as compared to the undoped TiO<sub>2</sub> (see also the arrow accounting for that shift in the  
236 inset of Fig. S1). This behavior confirms the photocatalytic activity enhancement in terms of  
237 ability to absorb the visible light. The decrease in  $E_g$  did not follow a progressive decay pattern,

238 which may be attributed to oxygen vacancies appearing on the surface of the Ru-doped TiO<sub>2</sub>  
239 nanotubes. Their irregular presence in the TiO<sub>2</sub> network affected the formation of the energy  
240 levels above the VB of TiO<sub>2</sub> and hence, the continuous rise in Ru concentration did not ensure  
241 an ever-decreasing  $E_g$  (within the ranged under study) (Nair et al., 2017). In fact, the Ru(0.15  
242 wt.%) -doped TiO<sub>2</sub> sample showed the highest  $E_g$  among all the doped materials. Nonetheless,  
243 even this sample was more active to visible light than the undoped TiO<sub>2</sub>.

244 The photoelectrochemical characterization of the undoped and Ru-doped TiO<sub>2</sub> nanotube  
245 arrays was carried out, since it is a very useful technique to know if charge separation can be  
246 promoted upon the application of  $E_{bias}$  to the illuminated semiconductor. If this is demonstrated,  
247 the degradation ability of PC may be upgraded by working under PEC conditions. The PEC  
248 process involves electron transfer across the semiconductor/electrolyte interface, a redox  
249 reaction and transient photocurrent flow. Transient photocurrent responses of all the  
250 photoanodes were recorded by linear sweep voltammetry in 0.050 M NaSO<sub>4</sub> at pH 1.0 under  
251 UV (Fig. 4a) and visible light (Fig. 4b) irradiation. As depicted, the photoanode potential was  
252 scanned from -0.3 V to +1.0 V, at a scan rate of 10 mV/s. A test carried out in the dark showed  
253 a low transient current flow between -0.3 V and +0.9 V, but it increased at  $E > +0.9$  V as a  
254 result of water oxidation to oxygen. Upon illumination either with UV or visible light, an anodic  
255 photocurrent transient ( $I_{ph}$ ) was observed, owing to the generation of photoinduced  $e^-_{CB}/h^+_{VB}$   
256 pairs via reaction (1). As a result, the production of TiO<sub>2</sub>(•OH) stimulated by  $h^+_{VB}$  from reaction  
257 (2) was feasible (Georgieva et al., 2012).

258 A saturation transient photocurrent (SP) at potentials  $> +0.5$  V is observed for the undoped  
259 TiO<sub>2</sub> photoanode illuminated with UV light (Fig. 4a). Conversely, an almost null photocurrent  
260 resulted within the whole potential range using visible light (Fig. 4b). Such behavior was  
261 expected due to the poor photoactivity of raw TiO<sub>2</sub> attributed under visible light. The Ru-doped  
262 TiO<sub>2</sub> photoanodes behaved differently, yielding a peak photocurrent (PP) at potentials around

263 -0.19 V and an SP at  $E > +0.5$  V upon irradiation with both light sources. With UV light, the  
264 magnitude of the SP for all the Ru-TiO<sub>2</sub> photoanodes was lower than that of the undoped TiO<sub>2</sub>  
265 (Fig. 4a). Based on this, it is expected that using UV the photoelectrocatalytic activity of the  
266 pure TiO<sub>2</sub> photoanode at  $E_{\text{bias}}$  corresponding to the SP domain will be higher than that achieved  
267 by the Ru-TiO<sub>2</sub> photoanodes. The opposite was observed in trials with visible light. The  
268 transient current values for all the Ru-TiO<sub>2</sub> samples were higher than that of the undoped TiO<sub>2</sub>  
269 (Fig. 4b). This is in agreement with the aforementioned red-shift found for the  $E_g$  upon Ru  
270 doping (i.e., decrease from 3.06 eV to 2.84-3.00 eV, Fig. S1).

271 Fig. 4a also reveals that, under irradiation with UV light, the PP value became greater as  
272 the Ru content in the impregnation solution was increased up to 0.10 wt.%, thereby decreasing  
273 for the photoanode with 0.15 wt.% Ru. This latter negative effect on the photocurrent transient  
274 can be attributed to the interfacial interaction between mixed oxides, since the electronic effects  
275 expected for TiO<sub>2</sub> can be partially isolated underneath excessively thick RuO<sub>2</sub> overlayers (Li et  
276 al., 2018). Moreover, the voltammograms became broader as the Ru content reached 0.08, 0.10  
277 and 0.15 wt.%, leading to a greater transient photocurrent at potentials before the one  
278 corresponding to the SP for the undoped TiO<sub>2</sub>. Accordingly, a higher photoelectrocatalytic  
279 activity of these Ru-TiO<sub>2</sub> photoanodes can be hypothesized at an anode potential within the  
280 range  $-0.234 \text{ V} < E_{\text{bias}} < +0.550 \text{ V}$  using UV light. Worth reminding, this applied  $E_{\text{bias}}$  minimizes  
281 the recombination of the photogenerated  $e^-_{\text{CB}}/h^+_{\text{VB}}$  pairs (Jiang et al., 2003). This is also valid  
282 under irradiation with visible light, although the transient photocurrents were narrower (Fig.  
283 4b). The trends with that lamp were analogous to those of Fig. 4a, showing a PP increase with  
284 Ru content rising from 0.005 to 0.10 wt.%. As mentioned above, this trend agrees with the red-  
285 shift observed for the  $E_g$  upon Ru doping (Fig. S1). For the Ru(0.15 wt.%) -doped TiO<sub>2</sub>, the PP  
286 value decreased and became similar to that of the Ru(0.04 wt.%) - and Ru(0.08 wt.%) -doped  
287 TiO<sub>2</sub>. Therefore, it is expected that all the Ru-TiO<sub>2</sub> photoanodes will show a higher

288 photoelectrocatalytic activity as compared to the undoped TiO<sub>2</sub> anode using visible light within  
289 the selected potential range. Similarly, the applied  $E_{\text{bias}}$  will minimize the recombination of the  
290 photogenerated  $e^-_{\text{CB}}/h^+_{\text{VB}}$  pairs, thereby upgrading the performance of PEC as compared to PC  
291 (Elsalamony and Mahmoud, 2017; Ismael, 2019).

### 292 3.2. Photoelectrocatalytic decolorization of the dye solution: effect of Ru doping

293 The performance of PC and PEC processes with the undoped and Ru-doped TiO<sub>2</sub> nanotube  
294 array photoanodes was studied from the color removal of 0.011 mM Terasil Blue dye solution  
295 containing 0.050 M NaSO<sub>4</sub> at pH 1.0, using UV or visible light to irradiate the anode. Based on  
296 the transient photocurrents described in the previous subsection, a positive effect of Ru doping  
297 in terms of photocatalytic degradation ability might be expected in PEC at  $E_{\text{bias}}$  matching with  
298 the PP potential (= -0.2 V) under UV or visible light, or at  $E_{\text{bias}}$  matching with the SP potential  
299 (= +0.6 V) under visible light. Therefore, these were the anodic potential values tested in PEC,  
300 whereas no potential was applied in PC, as depicted in Fig. 5.

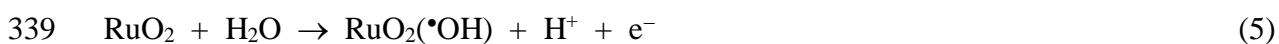
301 Fig. 5a shows the performance of the PC process (no applied  $E_{\text{bias}}$ ) with UV light, evaluated  
302 from the percentage of color removal determined via Eq. (4). The photocatalyst with the lowest  
303 Ru doping (0.005 wt.%) yielded a greater final decolorization than the undoped TiO<sub>2</sub> (92% vs  
304 90% at 120 min), being the color removal especially faster during the first 60 min. In fact, this  
305 Ru content was almost revealed as the optimum one to decolorize the Terasil Blue solutions,  
306 considering both the color removal rate and the decolorization percentage finally attained. The  
307 slowest and poorest (72% at 120 min) color disappearance was observed with 0.02 wt.% Ru.  
308 The photocatalysts doped with 0.04-0.10 wt.% Ru behaved similarly to the undoped TiO<sub>2</sub>,  
309 although a slightly higher color removal was achieved at 120 min with 0.08 wt.% Ru. Then, a  
310 clearly worse performance was found using the Ru(0.15wt.%) -doped TiO<sub>2</sub>. Ruthenium atoms  
311 doped on TiO<sub>2</sub> are expected to act as active sites that reduce the recombination rate of the  
312 photoinduced  $e^-_{\text{CB}}/h^+_{\text{VB}}$  pairs during the photocatalytic reaction, with the subsequent higher

313 production of  $\text{TiO}_2(\bullet\text{OH})$  that enhances the Terasil Blue degradation (Choi et al., 1994; Gaya  
314 and Abdullah, 2008). This is evident at 0.005 wt.% Ru. However, it seems that larger Ru  
315 contents became excessive and turned out to be detrimental in PC. This is explained by the  
316 probable role of Ru as a recombination center, as well as the partial hindrance to UV photons  
317 that cannot reach the  $\text{TiO}_2$  semiconductor (Choi et al., 1994; Nguyen-Phan et al., 2016).

318 The PC treatment of the dye solution was much less effective using visible light, as depicted  
319 in Fig. 5b, with all the photocatalysts leading to a slower decolorization rate and yielding a poor  
320 final color removal lower than 32%. In this system, all the Ru contents higher than 0.005 wt.%  
321 were beneficial as compared to the undoped  $\text{TiO}_2$ , in contrast to that observed in Fig. 5a. This  
322 confirms the positive effect of Ru doping to promote the visible-light photoactivity, ending in  
323 a greater production of  $\text{TiO}_2(\bullet\text{OH})$ . The optimum PC treatment with visible light was reached  
324 with the Ru(0.08 wt.%)-doped  $\text{TiO}_2$  photocatalyst. Again, an excessively high amount of Ru  
325 was detrimental due to its role as a recombination center (Gaya and Abdullah, 2008;  
326 Elsalamony and Mahmoud, 2017; Ismael, 2019).

327 The PEC activity of the same photocatalysts with UV light was then compared by using  
328 them as photoanodes, at  $E_{\text{bias}} = +0.6$  V (Fig. 5c and 5d, respectively) and  $E_{\text{bias}} = -0.2$  V (Fig. 5e  
329 and 5f, respectively). At +0.6 V, a negative influence of Ru doping was observed (Fig. 5c),  
330 since the greatest decolorization percentage was attained with the undoped  $\text{TiO}_2$  photoanode  
331 (91% at 120 min). Among the profiles found with the Ru-doped photoanodes, no substantial  
332 differences were observed, always reaching a lower color removal of 78-82%. The Ru(0.15  
333 wt.%)-doped  $\text{TiO}_2$  photoanode was an exception because the final color loss was analogous to  
334 that attained with the undoped  $\text{TiO}_2$ , although at much slower decolorization rate. These PEC  
335 results are in good agreement with the higher SP value associated to the undoped  $\text{TiO}_2$  as  
336 compared to all the Ru-doped photoanodes, except the one with 0.15 wt.% (see Fig. 4a). Worth

337 noting, in the case of the highest Ru doping, the possibility of •OH formation from the anodic  
338 oxidation reaction (5) if RuO<sub>2</sub> is present cannot be discarded:



340 where RuO<sub>2</sub>(•OH) denotes a physisorbed hydroxyl radical, analogous to that formed at the TiO<sub>2</sub>  
341 sites via reaction (3) but with greater oxidation ability (Panizza and Cerisola, 2009). The high  
342 oxidation power of this type of radical formed on the surface of dimensionally stable anodes  
343 has been confirmed by several authors (Panizza and Cerisola, 2009; Lanzalaco et al., 2018).

344 From the previous paragraph, it can be concluded that PEC at  $E_{\text{bias}} = +0.6$  V was less  
345 effective than PC when UV light was employed. A similar negative effect of Ru doping was  
346 verified using the same lamp but applying an  $E_{\text{bias}} = -0.2$  V (Fig. 5e). The undoped TiO<sub>2</sub>  
347 exhibited the highest decolorization power up to 60 min. However, at longer reaction time, the  
348 photoanodes doped with 0.10 and 0.15 wt.% Ru outperformed the undoped one, attaining a  
349 96% and 98% color removal at 120 min, respectively, vs 90% reached with raw TiO<sub>2</sub>.  
350 Therefore, working at  $E_{\text{bias}} = E(\text{PP})$  was favorable when more than 0.10 wt.% Ru was employed,  
351 being the Ru(0.15 wt.%)-doped TiO<sub>2</sub> the optimum photoanode. Otherwise, using the UV lamp,  
352 the PC treatment with the undoped TiO<sub>2</sub> photocatalyst was the best option to decolorize the dye  
353 solution.

354 The influence of Ru doping was opposite in PEC with visible light, as shown in Fig. 5d  
355 and 5f applying an  $E_{\text{bias}}$  of +0.6 or -0.2 V, respectively. In both cases, the undoped TiO<sub>2</sub>  
356 photoanode exhibited the lowest photoactivity, in agreement with its limited absorption in the  
357 visible range. The general trend was that an increase in the Ru content led to a larger  
358 decolorization, with the Ru(0.15 wt.%)-doped TiO<sub>2</sub> photoanode attaining the greatest  
359 percentage of color removal at 120 min (i.e., 28% and 36% at +0.6 or -0.2 V, respectively),  
360 although some composition did not agreed perfectly (see for example the 0.10 wt.% Ru content  
361 in Fig. 5f). As occurred in PEC with UV light, the photoanode synthesized with 0.15 wt.% Ru

362 was proven to be the optimum one. A comparison of the three systems with visible light (Fig.  
363 5b, 5d and 5f) also allows concluding that PEC with 0.15 wt.% Ru at  $E(PP)$  as the applied  
364 potential was the most convenient treatment to decolorize the dye solution. Clearly, PEC was  
365 more effective than PC when Ru-doped  $TiO_2$  photoanodes were employed under visible light,  
366 which corroborates that the applied potential is crucial to minimize the capture of  $e^-_{CB}$  by  
367 photoholes (Jiang et al., 2003). As a result, a greater production of  $TiO_2(\cdot OH)$  was achieved,  
368 accounting for a more significant decolorization (Choi et al., 1994; Gaya and Abdullah, 2008).

### 369 *3.3. Photoelectrocatalytic decolorization of dye solution: effect of thermal treatment and pH*

370 Fig. S2 shows the transient photocurrent responses recorded by linear sweep voltammetry  
371 within the potential range between -0.5 and +1.0 V using the Ru(0.15 wt.%)-doped  $TiO_2$   
372 photoanode as working electrode, annealed at different temperatures after doping. The analyses  
373 were made in 0.050 M  $NaSO_4$  solutions at different pH, using UV or visible light. The curve  
374 obtained from a comparative trial in the dark is also exemplified (similar results were obtained  
375 in all the dark experiments). Clearly, pH values higher than 1.0 and annealing temperatures  
376 higher than 200 °C led to a significant decrease of the magnitude of the current values, as  
377 compared to trials at pH 1.0 and 200 °C that showed a PP and SP regardless of the type of light.  
378 The decrease in the photocurrent magnitude as the annealing temperature was increased can be  
379 attributed to the varying presence of residual chloride or protons on the  $TiO_2$  substrate (Siviglia  
380 et al., 1983). Also, a greater residual hydration (which is related to the presence of chemically  
381 bound water in the bulk) of the Ru- $TiO_2$  lattice can be associated with the lower annealing  
382 temperatures, thereby affecting the point of zero charge (pzc) of the surface oxide because it  
383 has influence on the behavior of the whole phase and affects its acid-base properties (Parks and  
384 de Bruyn, 1962; Siviglia et al., 1983; Ardizzone et al., 1989). According to Siviglia et al. (1983),  
385 the pzc value decreases as the synthesis temperature decreases. The variation of the pzc value  
386 with the temperature of preparation was interpreted in terms of change in the cation-anion

387 spacing in the lattice due to residual chloride, which was dependent on the temperature of  
388 decomposition of  $\text{RuCl}_3$ . Thus, it is evident that the nature of the anode surface sites depends  
389 to a large extent on the method of preparation and annealing temperature treatment (Siviglia et  
390 al., 1983). The solution pH has also a close relationship with the pzc. The anode presents surface  
391 adsorption sites that become positively charged upon proton adsorption (at  $\text{pH} < \text{pzc}$ ), or  
392 negatively charged upon proton desorption ( $\text{pH} > \text{pzc}$ ). The anode surface has no net charge at  
393  $\text{pH} = \text{pzc}$  (Parks and de Bruyn, 1962). According to Fig. S2, the photocurrent response was  
394 highly enhanced at pH 1.0 when the anode was prepared at 200 °C, which means that the surface  
395 was positively charged. This is deduced from the fact that the anode surface was probably a  
396 mixture of  $\text{TiO}_2 + \text{RuO}_2$ , where the former oxide (with  $\text{pzc} = 6$ ) was predominant (Subramanian  
397 et al., 1989; Sugimoto and Zhou, 2002). In contrast, the negatively charged surface appearing  
398 at pH 7.0 and pH 9.0 was less favorable to photocurrent flow in the Ru-doped  $\text{TiO}_2$  anode.

399 The same optimized  $\text{TiO}_2$  photocatalyst, i.e. that with 0.15 wt.% Ru, was employed to  
400 decolorize the 0.011 mM dye solution by PC. The highest color removal was obtained at  
401 annealing temperature of 200 °C and pH 9.0 (close to pH 1.0), either with UV (Fig. 6a) or  
402 visible (Fig. 6b) light. Using the photocatalyst annealed at that temperature, the effect of pH on  
403 the decolorization performance was as follows:  $\text{pH } 9.0 > \text{pH } 1.0 \geq \text{pH } 7.0$ . This means that in  
404 PC the adsorption of the dye molecules was enhanced as the photocatalyst surface became more  
405 negatively charged. When the solution pH was fixed to 1.0, a negative influence of rising  
406 annealing temperature was found because the decolorization decayed in the order:  $200 \text{ °C} >$   
407  $450 \text{ °C} \geq 600 \text{ °C}$ . The use of 600 °C was highly detrimental regardless of the light source, which  
408 confirms the high relevance of the surface hydration to explain the photocatalytic activity.

409 As can be seen in Fig. 7, the PEC treatments presented a greater effectiveness as compared  
410 to the corresponding PC assays of Fig. 6, ending in a larger decolorization at 120 min due to  
411 the minimized destruction of charge carriers (Jiang et al., 2003). Also, the effect of pH and

412 annealing temperature was different to that commented for PC. The best conditions for  
413 decolorization, both with UV (Fig. 7a) and visible light (Fig. 7b), were 200 °C and pH 1.0,  
414 applying an  $E_{\text{bias}} = E(\text{PP}) = -0.2$  V. Note that in the trials with visible light, a more powerful  
415 lamp was employed as compared to the assays discussed in Fig. 5f, which led to a greater final  
416 decolorization (55% instead of 36%). The results with both lamps agreed perfectly with the  
417 profiles described in Fig. S2, with the maxima appearing under those conditions (i.e., PP  
418 potential). The use of  $E_{\text{bias}} = E(\text{SP}) = +0.6$  V affected negatively to the oxidation power, but  
419 still led to the second strongest PEC treatment, either with UV or visible light. This means that  
420 the annealing temperature and pH certainly were the most influential parameters. When the  $E_{\text{bias}}$   
421 was fixed at  $E(\text{SP})$ , the following trends were observed: (i) with UV light and the samples made  
422 at 200°C, a much lower and close percentage of color removal was attained as pH 1.0 and pH  
423 9.0; and (ii) with visible light at pH 1.0, the worse performance was clearly found at 600 and  
424 450 °C. These results evidence that the annealing temperature after the Ru impregnation and  
425 the pH of the dye solution played an important role in the photocatalytic activity of the Ru-  
426 doped TiO<sub>2</sub> photoanodes.

427 The stability and reusability have been tested by recording transient photocurrent responses  
428 using the Ru(0.15 wt.%) -doped TiO<sub>2</sub> nanotube array photoanode under UV illumination in a  
429 0.050 M Na<sub>2</sub>SO<sub>4</sub> solution at pH 1.0, as shown in Fig. S3. The photocurrent values were recorded  
430 at 0 h (fresh electrode) and at different times of use from 0 to 28 h (considering PEC trials with  
431 a duration of 2 h each). The main change is observed in the peak photocurrent value, which  
432 decreased as the photoanode was successively re-used in PEC. Since the percentage of color  
433 removal at 120 min employing  $E_{\text{bias}} = -0.2$  V decreased from 98% after a single use (i.e., 2 h)  
434 to ~80% after fourteen uses (i.e., 28 h), it was concluded that the photoanode should be  
435 discarded after five cycles of 120 min.

#### 436 **4. Conclusions**

437 It has been shown that Terasil Blue dye can be gradually oxidized by PC and PEC with  
438 Ru-doped TiO<sub>2</sub> nanotube arrays as photoanodes upon irradiation with UV or visible light. The  
439 effect of the Ru content (0.005-0.15 wt.%) and annealing temperature (200-650 °C) employed  
440 to synthesize the photocatalysts, as well as of the solution pH (1.0-9.0) and  $E_{\text{bias}}$  fixed in PEC  
441 on the color removal was investigated in detail. The optimum decolorization was achieved in  
442 PEC treatment with the Ru(0.15 wt.%, 200 °C)-doped TiO<sub>2</sub> photoanode at  $E_{\text{bias}} = -0.2$  V using  
443 UV light, attaining a 98% color removal at 120 min for a 0.011 mM dye solution at pH 1.0.  
444 This is accounted for by the positive influence of the applied  $E_{\text{bias}}$ , which reduced the  
445 recombination rate of the photoinduced  $e^-_{\text{CB}}/h^+_{\text{VB}}$  pairs, eventually yielding a larger amount of  
446 adsorbed  $\bullet\text{OH}$  as compared to PC process. The surface analyses of the synthesized photoanodes  
447 revealed the predominance of the anatase phase, with a minor presence of rutile. A smaller  
448 nanotube diameter was observed as the Ru content was increased. The Ru doping caused a red-  
449 shift, with the  $E_{\text{gap}}$  decreasing from 3.06 to less than 3.0 eV depending on the Ru content. The  
450 visible-light photoactivity promoted upon Ru doping opens the door to the use of the  
451 synthesized photoanodes in solar PEC, since sunlight acts as a source of combined UV/Vis  
452 radiation.

#### 453 **Acknowledgements**

454 P. García-Ramírez is grateful to the National Council for Science and Technology  
455 (CONACYT, Mexico) for the PhD scholarship granted. The authors also thank the funding  
456 from projects CTQ2016-78616-R (AEI/FEDER, EU) and PID2019-109291RB-I00 (AEI,  
457 Spain).

458 **References**

- 459 Anandan, S., Ponnusamy, V.K., Ashokkumar, M., 2020. A review on hybrid techniques for the  
460 degradation of organic pollutants in aqueous environment. *Ultrason. Sonochem.* 67,  
461 105130.
- 462 Ardizzone, S., Daggetti, A., Franceschi, L., Trasatti, S. 1989. The point of zero charge of  
463 hydrous RuO<sub>2</sub>. *Coll. Surfaces* 35, 85-96.
- 464 Arsov, L.D., Kormann, C., Plieth, W., 1991. Electrochemical synthesis and *in situ* Raman  
465 spectroscopy of thin films of titanium dioxide. *J. Raman Spectrosc.* 22, 573-575.
- 466 Basavarajappa, P.S., Patil, S.B., Ganganagappa, N., Reddy, K.R., Raghu, A.V., Reddy, Ch.V.,  
467 2020. Recent progress in metal-doped TiO<sub>2</sub>, non-metal doped/codoped TiO<sub>2</sub> and TiO<sub>2</sub>  
468 nanostructured hybrids for enhanced photocatalysis. *Int. J. Hydrogen Energy* 45, 7764-  
469 7778.
- 470 Bessegato, G.G., Guaraldo, T.T., de Brito, J.F., Brugnera, M.F., Zanoni, M.V.B., 2015.  
471 Achievements and trends in photoelectrocatalysis: from environmental to energy  
472 applications. *Electrocatalysis* 6, 415-441.
- 473 Brillas, E., Martínez-Huitle, C.A., 2015. Decontamination of wastewaters containing synthetic  
474 organic dyes by electrochemical methods. An updated review. *Appl. Catal. B: Environ.*  
475 166-167, 603-643.
- 476 Brillas, E., Sirés, I., Oturan, M.A., 2009. Electro-Fenton process and related electrochemical  
477 technologies based on Fenton's reaction chemistry. *Chem. Rev.* 109, 6570-6631.
- 478 Chahmana, N., Matrakova, M., Zerroual, L., Pavlov, D., 2009. Influence of some metal ions on  
479 the structure and properties of doped  $\beta$ -PbO<sub>2</sub>. *J. Power Sources* 191, 51-57.
- 480 Changanqui, K., Brillas, E., Alarcón, H., Sirés, I., 2020. ZnO/TiO<sub>2</sub>/Ag<sub>2</sub>Se nanostructures as  
481 photoelectrocatalysts for the degradation of oxytetracycline in water. *Electrochim. Acta*  
482 331, 135194.

483 Chen, D., Cheng, Y., Zhou, N., Chen, P., Wang, Y., Li, K., Huo, S., Cheng, P., Peng, P., Zhang,  
484 R., Wang, L., Liu, H., Liu, Y., Ruan, R., 2020. Photocatalytic degradation of organic  
485 pollutants using TiO<sub>2</sub>-based photocatalysts: A review. *J. Clean. Prod.* 268, 121725.

486 Choi, W., Termin, A., Hoffmann, M.R., 1994. The role of metal ion dopants in quantum-sized  
487 TiO<sub>2</sub>: Correlation between photoreactivity and charge carrier recombination dynamics. *J.*  
488 *Phys. Chem.* 98, 13669-13679.

489 Choo, G., Wang, W., Cho, H.-S., Kim, K., Park, K., Oh, J.-E., 2020. Legacy and emerging  
490 persistent organic pollutants in the freshwater system: Relative distribution,  
491 contamination trends, and bioaccumulation. *Environ. Int.* 135, 105377.

492 Clematis, D., Cerisola, G., Panizza, M., 2017. Electrochemical oxidation of a synthetic dye  
493 using a BDD anode with a solid polymer electrolyte. *Electrochem. Commun.* 75, 21-24.

494 Cornejo, O., Murrieta, M.F., Castañeda, L.F., Nava, J.L., 2020. Characterization of the reaction  
495 environment in flow reactors fitted with BDD electrodes for use in electrochemical  
496 advanced oxidation processes: A critical review. *Electrochim. Acta* 331, 135373.

497 Daghrrir, R., Drogui, P., Robert, D., 2012. Photoelectrocatalytic technologies for environmental  
498 applications. *J. Photochem. Photobiol. A: Chem.* 238, 41-52.

499 Elsalamony, R.A., Mahmoud, S.A., 2017. Preparation of nanostructured ruthenium doped  
500 titania for the photocatalytic degradation of 2-chlorophenol under visible light. *Arab. J.*  
501 *Chem.* 10, 194-205.

502 Espinola-Portilla, F., Navarro-Mendoza, R., Gutiérrez-Granados, S., Morales-Muñoz, U.,  
503 Brillas-Coso, E., Peralta-Hernández, J.M., 2017. A simple process for the deposition of  
504 TiO<sub>2</sub> onto BDD by electrophoresis and its application to the photoelectrocatalysis of Acid  
505 Blue 80 dye. *J. Electroanal. Chem.* 802, 57-63.

506 Gaya, U.I., Abdullah, A.H., 2008. Heterogeneous photocatalytic degradation of organic  
507 contaminants over titanium dioxide: A review of fundamentals, progress and problems.  
508 J. Photochem. Photobiol. C: Photochem. Rev. 9, 1-12.

509 Georgieva, J., Valova, E., Armyanov, S., Philippidis, N., Poulios, I., Sotiropoulos, S., 2012. Bi-  
510 component semiconductor oxide photoanodes for the photoelectrocatalytic oxidation of  
511 organic solutes and vapours: A short review with emphasis to TiO<sub>2</sub>-WO<sub>3</sub> photoanodes. J.  
512 Hazard. Mater. 211-212, 30-46.

513 González, A.S., Solis-Cortazar, J.C., Pineda-Arellano, C.A., Ramírez-Morales, E., de los  
514 Monteros, A.E., Silva-Martínez, S., 2019. Synthesis of ruthenium-doped TiO<sub>2</sub> nanotube  
515 arrays for the photocatalytic degradation of Terasil Blue dye. J. Nanosci. Nanotechnol.  
516 19, 5211-5219.

517 Hernández, R., Olvera-Rodríguez, I., Guzmán, C., Medel, A., Escobar-Alarcón, L., Brillas, E.,  
518 Sirés, I., Esquivel, K., 2018. Microwave-assisted sol-gel synthesis of an Au-TiO<sub>2</sub>  
519 photoanode for the advanced oxidation of paracetamol as model pharmaceutical  
520 pollutant. Electrochem. Commun. 96, 42-46.

521 Ismael, M., 2019. Highly effective ruthenium-doped TiO<sub>2</sub> nanoparticles photocatalyst for  
522 visible-light-driven photocatalytic hydrogen production. New J. Chem. 43, 9596-9605.

523 Jiang, D., Zhao, H., Zhang, S., John, R., 2003. Characterization of photoelectrocatalytic  
524 processes at nanoporous TiO<sub>2</sub> film electrodes: Photocatalytic oxidation of glucose. J.  
525 Phys. Chem. B 107, 12774-12780.

526 Kanan, S., Moyet, M.A., Arthur, R.B., Patterson, H.H., 2020. Recent advances on TiO<sub>2</sub>-based  
527 photocatalysts toward the degradation of pesticides and major organic pollutants from  
528 water bodies. Catal. Rev. Sci. Eng. 62, 1-65.

529 Lanzalaco, S., Sirés, I., Galia, A., Sabatino, M.A., Dispenza, C., Scialdone, O., 2018. Facile  
530 crosslinking of poly(vinylpyrrolidone) by electro-oxidation with IrO<sub>2</sub>-based anode under  
531 potentiostatic conditions. *J. Appl. Electrochem.* 48, 1343-1352.

532 Li, H., Zha, S., Zhao, Z.-J., Tian, H., Chen, S., Gong, Z., Cai, W., Wang, Y., Cui, Y., Zeng, L.,  
533 Mu, R., Gong, J., 2018. The nature of loading-dependent reaction barriers over mixed  
534 RuO<sub>2</sub>/TiO<sub>2</sub> catalysts. *ACS Catal.* 8, 5526-5532.

535 López, R., Gómez, R., 2012. Band-gap energy estimation from diffuse reflectance  
536 measurements on sol-gel and commercial TiO<sub>2</sub>: A comparative study. *J. Sol Gel Sci.*  
537 *Technol.* 61, 1-7.

538 Ma, H.L., Yang, J.Y., Dai, Y., Zhang, Y.B., Lu, B., Ma, G.H., 2007. Raman study of phase  
539 transformation of TiO<sub>2</sub> rutile single crystal irradiated by infrared femtosecond laser. *Appl.*  
540 *Surf. Sci.* 253, 7497-7500.

541 Martínez-Huitle, C.A., Rodrigo, M.A., Sirés, I., Scialdone, O., 2015. Single and coupled  
542 electrochemical processes and reactors for the abatement of organic water pollutants: A  
543 critical review. *Chem. Rev.* 115, 13362-13407.

544 Nair, R.G., Mazumdar, S., Modak, B., Bapat, R., Ayyub, P., Bhattacharyya, K., 2017. The role  
545 of surface O-vacancies in the photocatalytic oxidation of Methylene Blue by Zn-doped  
546 TiO<sub>2</sub>: A Mechanistic approach. *J. Photochem. Photobiol. A: Chem.* 345, 36-53.

547 Nguyen-Phan, T.D., Luo, S., Vovchok, D., Llorca, J., Sallis, S., Kattel, S., Xu, W., Piper, L.F.J.,  
548 Polyansky, D.E., Senanayake, S.D., Stacchiola, D.J., Rodríguez, J.A., 2016. Three-  
549 dimensional ruthenium-doped TiO<sub>2</sub> sea urchins for enhanced visible-light-responsive H<sub>2</sub>  
550 production. *Phys. Chem. Chem. Phys.* 18, 15972-15979.

551 Oriol, R., Sirés, I., Brillas, E., De Andrade, A.R., 2019. A hybrid  
552 photoelectrocatalytic/photoelectro-Fenton treatment of Indigo Carmine in acidic aqueous  
553 solution using TiO<sub>2</sub> nanotube arrays as photoanode. *J. Electroanal. Chem.* 847, 113088.

554 Ohno, T., Tanigawa, F., Fujihara, K., Izumi, S., Matsumura, M., 1999. Photocatalytic oxidation  
555 of water by visible light using ruthenium-doped titanium dioxide powder. *J. Photochem.*  
556 *Photobiol. A: Chem.* 127, 107-110.

557 Oturan, M.A., Aaron, J.J., 2014. Advanced oxidation processes in water/wastewater treatment:  
558 principles and applications. A review. *Crit. Rev. Environ. Sci. Technol.* 44, 2577-2641.

559 Panizza, M., Cerisola, G., 2009. Direct and mediated anodic oxidation of organic pollutants.  
560 *Chem. Rev.* 109, 6541-6569.

561 Parks, G.A., de Bruyn, P.L., 1962. The zero point of charge of oxides. *J. Phys. Chem.* 66, 967-  
562 973.

563 Peleyeju, M.G., Arotiba, O.A., 2018. Recent trend in visible-light photoelectrocatalytic systems  
564 for degradation of organic contaminants in water/wastewater. *Environ. Sci. Water Res.*  
565 *Technol.* 4, 1389-1411.

566 Secundino-Sánchez, O., Díaz-Reyes, J., Sánchez-Ramírez, J.F., Martínez-Juárez, J., 2019.  
567 Stimulation of the photoluminescent properties of electrospinning TiO<sub>2</sub> nanofibres  
568 induced by structural modifications resulting from annealing at high temperatures. *J*  
569 *Lumin.* 215, 116700.

570 Senthilnathan, M., Ho, D.P., Vigneswaran, S., Ngo, H.H., Shon, H.K., 2010. Visible light  
571 responsive ruthenium-doped titanium dioxide for the removal of metsulfuron-methyl  
572 herbicide in aqueous phase. *Sep. Purif. Technol.* 75, 415-419.

573 Shin, S., Kim, K., Choi, J., 2013. Fabrication of ruthenium-doped TiO<sub>2</sub> electrodes by one-step  
574 anodization for electrolysis applications. *Electrochem. Commun.* 36, 88-91.

575 Siviglia, P., Daggetti, A., Trasatti, S., 1983. Influence of the preparation temperature of  
576 ruthenium dioxide on its point of zero charge. *Coll. Surfaces* 7, 15-27.

577 So, S., Lee, K., Schmuki, P., 2012. Ru-doped TiO<sub>2</sub> nanotubes: Improved performance in dye-  
578 sensitized solar cells. *Phys. Status Solidi Rapid Res Lett.* 6,169-171.

579 Subramanian, S., Schwarz, J.A., Hejase, Z., 1989. The temperature dependence of the point of  
580 zero charge of  $\gamma$ -Al<sub>2</sub>O<sub>3</sub>, TiO<sub>2</sub>, and physical mixtures. *J. Catal.* 117, 512-518.

581 Sugimoto, T., Zhou, X., 2002. Synthesis of uniform anatase TiO<sub>2</sub> nanoparticles by the gel-sol  
582 method: 2. Adsorption of OH<sup>-</sup> ions to Ti(OH)<sub>4</sub> gel and TiO<sub>2</sub> particles. *J. Coll. Interface*  
583 *Sci.* 252, 347-353.

584 Thiam, A., Sirés, I., Garrido, J.A., Rodríguez, R.M., Brillas, 2015. Effect of anions on  
585 electrochemical degradation of azo dye Carmoisine (Acid Red 14) using a BDD anode  
586 and air-diffusion cathode. *Sep. Purif. Technol.* 140, 43-52.

587 Vasconcelos, V.M., Ponce-de-León, C., Nava, J.L., Lanza, M.R.V., 2016. Electrochemical  
588 degradation of RB-5 dye by anodic oxidation, electro-Fenton and by combining anodic  
589 oxidation–electro-Fenton in a filter-press flow cell. *J. Electroanal. Chem.* 765, 179-187.

590 Viswanathamurthi, P., Bhattarai, N., Kim, C.K., Kim, H.Y., Lee, D.R., 2004. Ruthenium doped  
591 TiO<sub>2</sub> fibers by electrospinning. *Inorg. Chem. Commun.* 7, 679-682.

592 Wang, Z., Liu, B., Xie, Z., Li, Y., Shen, Z.-Y., 2016. Preparation and photocatalytic properties  
593 of RuO<sub>2</sub>/TiO<sub>2</sub> composite nanotube arrays. *Ceram. Int.* 42, 13664-13669.

594 Yan, H., Wang, X., Yao, M., Yao, X., 2013. Band structure design of semiconductors for  
595 enhanced photocatalytic activity: The case of TiO<sub>2</sub>. *Progress Natural Sci.: Mater. Intern.*  
596 23, 402-407.

597 Zhang, Y., Xiong, X., Han, Y., Zhang, X., Shen, F., Deng, S., Xiao, H., Yang, X., Yang, G.,  
598 Peng, H., 2012. Photoelectrocatalytic degradation of recalcitrant organic pollutants using  
599 TiO<sub>2</sub> film electrodes: An overview. *Chemosphere* 88, 145-154.

600 Zhu, Y., Zhu, R., Xi, Y., Zhu, J., Zhu, G., He, H., 2019. Strategies for enhancing the  
601 heterogeneous Fenton catalytic reactivity: A review. *Appl. Catal. B: Environ.* 255,  
602 117739.

603

604 **Figure captions**

605 **Fig. 1.** SEM images of (a) undoped and (b-g) Ru-doped TiO<sub>2</sub> nanotube array photoanodes. The  
606 solutions for Ru impregnation contained: (b) 0.005, (c) 0.02, (d) 0.04, (e) 0.08, (f) 0.10 and (g)  
607 0.15 wt.% Ru. The annealing of the Ru-impregnated TiO<sub>2</sub> samples was made at 200 °C.

608 **Fig. 2.** X-ray diffractograms of undoped (curve *a*) and Ru-doped (curves *b-g*) TiO<sub>2</sub> nanotube  
609 array photoanodes. The Ru content in each impregnation solution and the annealing temperature  
610 are those mentioned in Fig. 1. Titanium (Ti), anatase (A) and rutile (R) peaks are assigned.

611 **Fig. 3.** Raman spectra of undoped (curve *a*) and Ru-doped (curves *b-g*) TiO<sub>2</sub> nanotube array  
612 photoanodes. The Ru content in each impregnation solution and the annealing temperature are  
613 those mentioned in Fig. 1.

614 **Fig. 4.** Linear sweep voltammograms of undoped and Ru-doped TiO<sub>2</sub> nanotube array anodes in  
615 a 0.050 M Na<sub>2</sub>SO<sub>4</sub> solution at pH 1.0, at a scan rate of 10 mV/s. The anode was illuminated  
616 with: (a) UV light (11SC-1 Pen-Ray lamp) and (b) visible light (two 25W LED lamps), although  
617 the current with the undoped anode in the dark is shown for comparison. The annealing of the  
618 Ru-impregnated TiO<sub>2</sub> samples was made at 200 °C. The potentials are referred to the Ag|AgCl  
619 (3 M KCl) reference electrode.

620 **Fig. 5.** Time course of color removal during the treatment of the solution containing 0.011 mM  
621 Terasil Blue dye and 0.050 M Na<sub>2</sub>SO<sub>4</sub> at pH 1.0, using the undoped and Ru-doped TiO<sub>2</sub>  
622 nanotube arrays. Process: (a,b) PC, (c,d) PEC at  $E_{\text{bias}} = +0.6$  V and (e,f) PEC at  $E_{\text{bias}} = -0.2$  V.  
623 The annealing of the Ru-impregnated TiO<sub>2</sub> samples was made at 200 °C. In plots (c-f), the  
624 potentials are referred to the Ag|AgCl (3 M KCl) reference electrode. The nanotubes were  
625 illuminated with: (a,c,e) UV light (11SC-1 Pen-Ray lamp) and (b,d,f) visible light (two 25W  
626 LED lamps).

627 **Fig. 6.** Influence of solution pH and annealing temperature on the evolution of color removal  
628 with time during the PC treatment of the solution containing 0.011 mM Terasil Blue dye and  
629 0.050 M Na<sub>2</sub>SO<sub>4</sub>, using the Ru(0.15 wt.%)-doped TiO<sub>2</sub> nanotube arrays illuminated with: (a)  
630 UV light (11SC-1 Pen-Ray lamp) and (b) visible light (50 W halogen MR16 LED lamp).

631 **Fig. 7.** (a) Influence of solution pH and annealing temperature on the evolution of color removal  
632 with time during the PEC treatment of the dye solution like that of Fig. 6. The Ru(0.15 wt.%)-  
633 doped photoanodes were illuminated with UV light, at  $E_{\text{bias}} = -0.2$  or  $+0.6$  V. (b) Influence of  
634 the annealing temperature for similar trials, at pH 1.0 using visible light (50 W halogen MR16  
635 LED lamp). All the potentials are referred to the Ag|AgCl (3 M KCl) reference electrode.

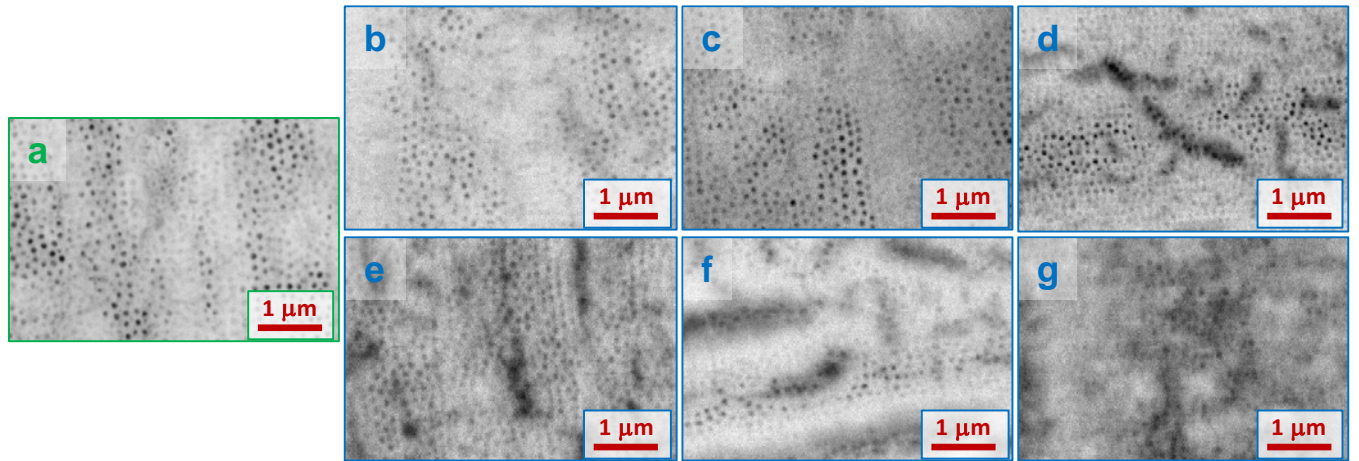


**Figure 1**

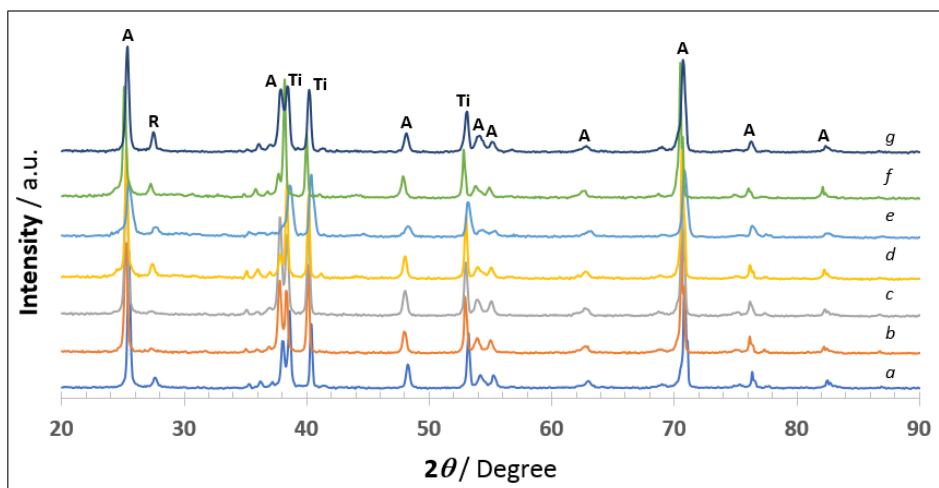


**Figure 2**

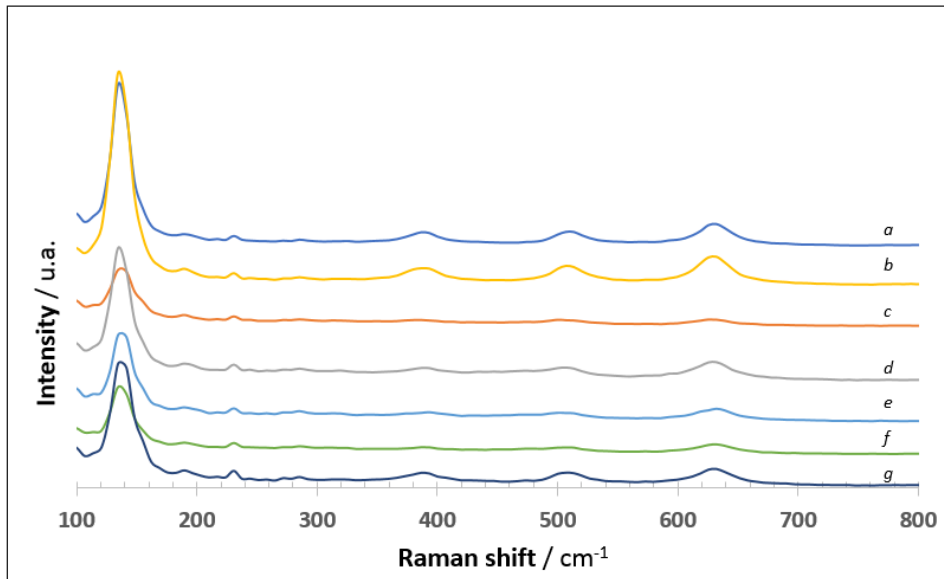


**Figure 3**

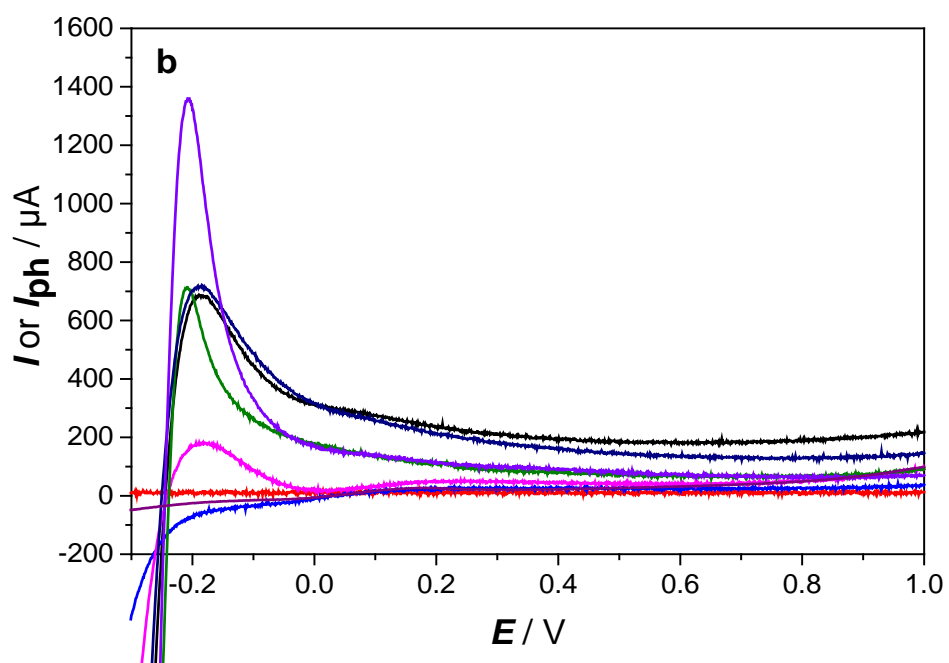
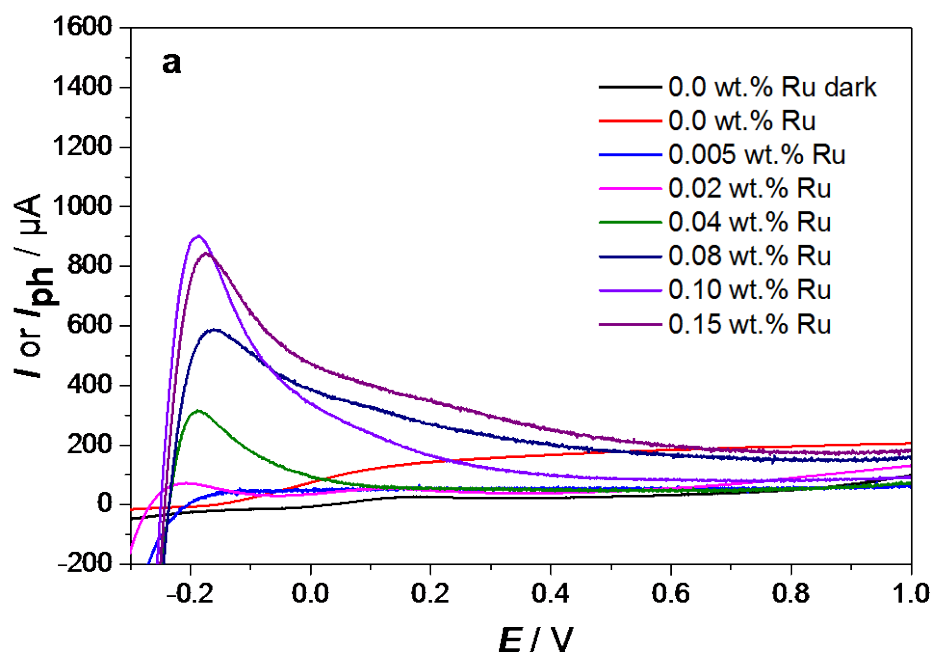


Figure 4

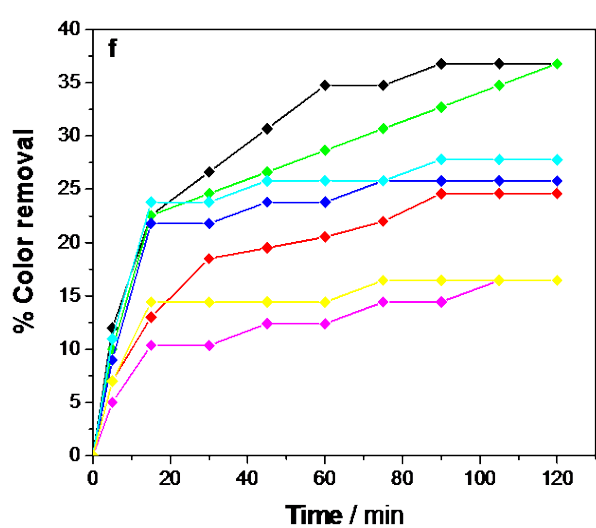
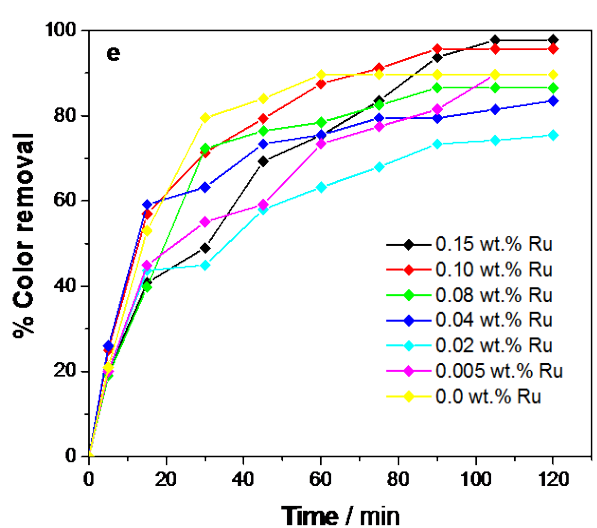
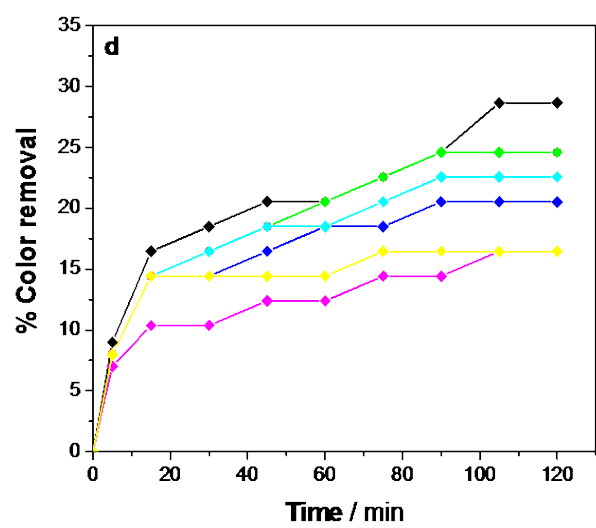
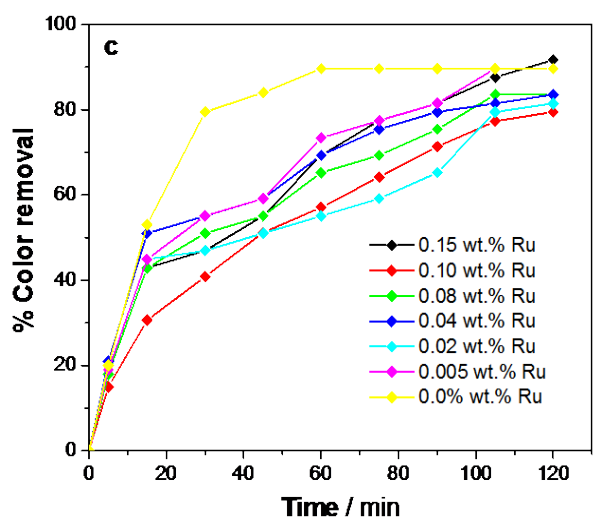
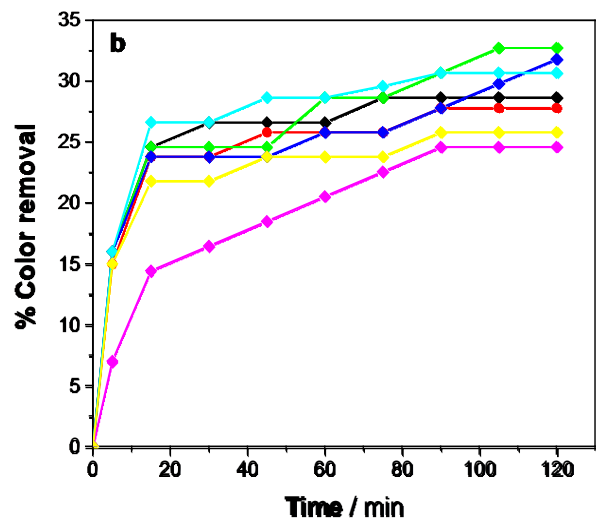
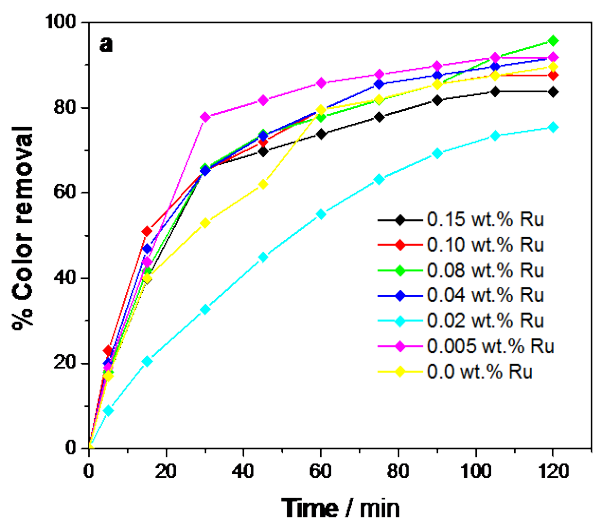
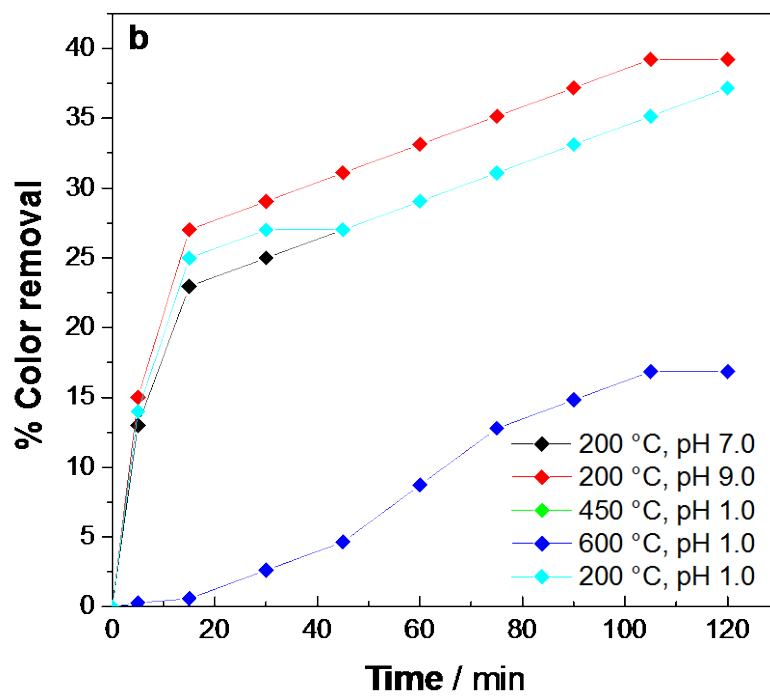
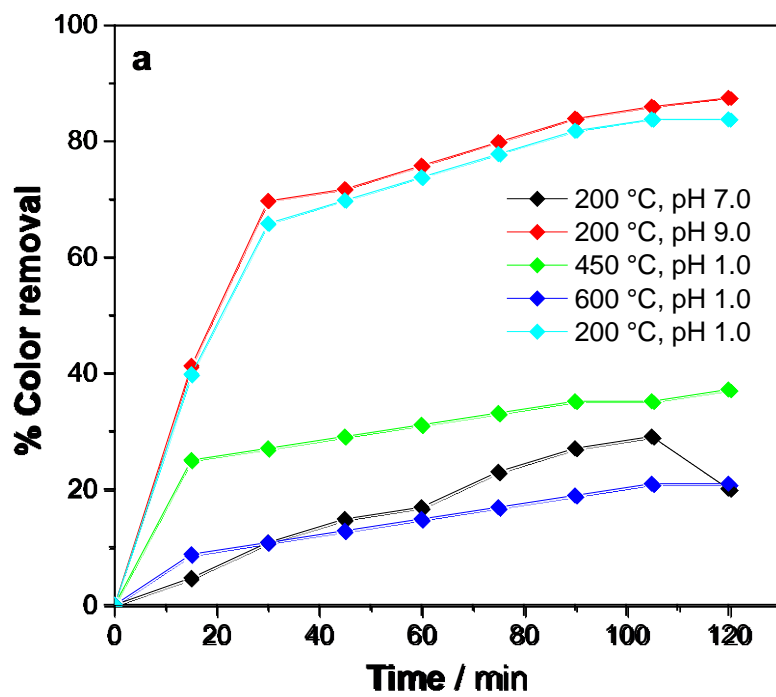


Figure 5



**Figure 6**

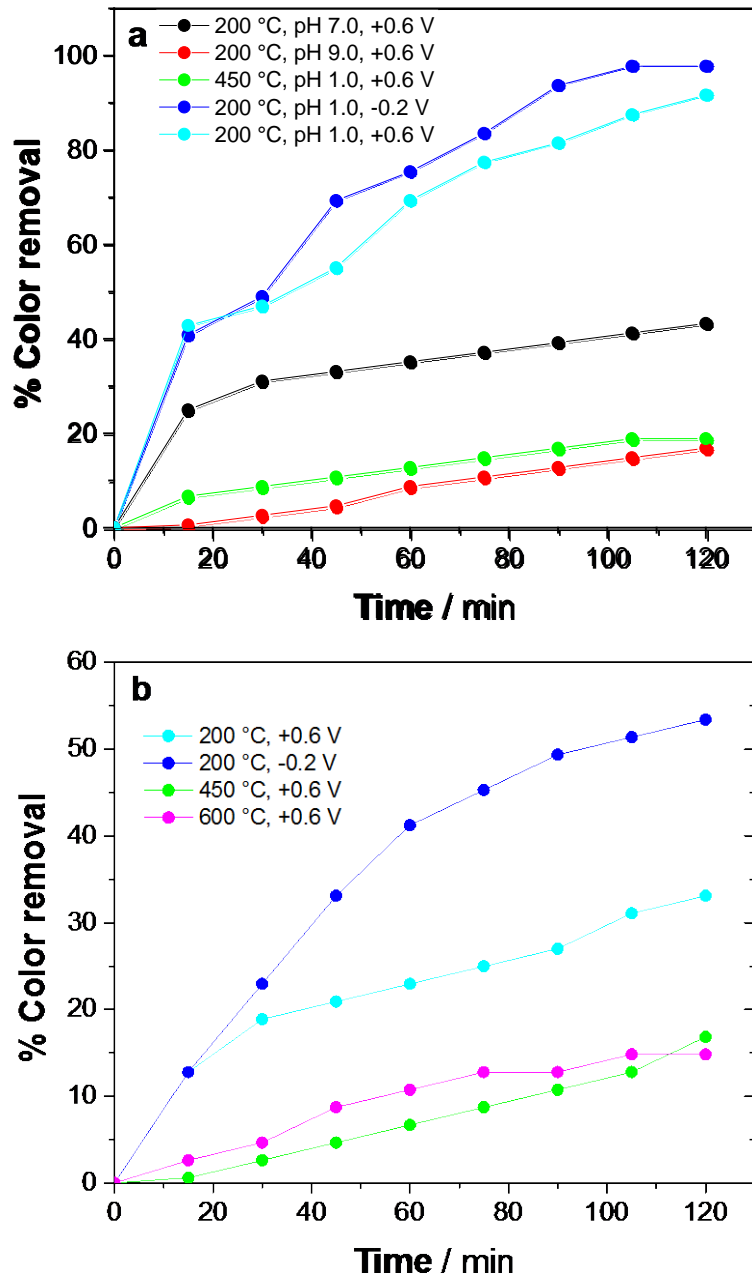


Figure 7